IEEE Access
Multidisciplinary | Rapid Review | Open Access Journal

Received September 20, 2018, accepted November 3, 2018, date of publication November 16, 2018,
date of current version December 19, 2018.

Digital Object Identifier 10.1109/ACCESS.2018.2881729

Mechanical Behaviors and Damage Constitutive Model of Thermally Treated Sandstone Under Impact Loading

TUBING YIN, PIN WANG, JIAN YANG, AND XIBING LI
School of Resources and Safety Engineering, Central South University, Changsha 410083, China

Corresponding authors: Tubing Yin (tubing_yin@mail.csu.edu.cn) and Pin Wang (wp8023csu@mail.csu.edu.cn)

This work was supported in part by the National Natural Science Foundation of China under Grant 51774325, in part by the State Key Program of National Natural Science Foundation of China under Grant 41630642, in part by the State Key Research Development Program of China under Grant 2016YFC0600706, in part by the Innovation-Driven Project of Central South University under Grant 2017CX006, and in part by the Hunan Provincial Natural Science Foundation of China under Grant 2017JJ3389.

ABSTRACT Thermal-mechanical coupling damage is an important factor leading to instability and failure of rock mass engineering. The constitutive relation and damage evolution of rock-like materials under high strain rate is crucial parameters for the design of underground rock mass structures, and is also an essential foundation for the analysis of instability phenomena in rock mass engineering. In this paper, a series of physical properties, static, and dynamic mechanical tests were carried out on Changsha sandstone after different high temperature treatments (ranging from 25 °C to 800 °C). Results indicate that thermal treatment effectively weakens the sandstone specimens. Under dynamic loading, the rock shows obvious strain rate effect, and the stress-strain curve changes from brittleness to viscoelasticity with the increase of temperature. Based on statistical damage theory and Weibull distribution, combining the analysis of the change laws of stress-strain curves of sandstone with temperature, a damage constitutive model that can reflect the variation in dynamic mechanical properties with temperature was proposed, for which the ultrasonic velocity is used to characterize the initial damage of rock caused by high temperature. Thereafter, the rationality of the constitutive model was verified by experiments. Combing damage evolution characteristics and rock failure process recorded by high-speed camera, the dynamic stress-strain relation curves of rock under different high temperature are divided into four stages, and the damage evolution process of rock under thermo-mechanical coupling was also analyzed. Results indicate that the values of thermo-mechanical damage increase exponentially with rock strain, and the damage evolution rate presents a two stage variation of first increase and then decrease. The initial damage stress of rock decreases with increasing temperature, but always maintains a stable percentage compared with the peak stress of the rock. Although the damage value at the peak point of stress increases with the increase of the temperature, it did not reach the maximum value of 1, which indicates that the rock damage continues to increase in the post peak loading stage. The findings of this paper can provide guidance for the macroscopic mechanical damage of rock under high temperatures and dynamic loading.

INDEX TERMS Constitutive model, damage evolution, dynamic properties, sandstone, thermal treatment.

I. INTRODUCTION

The mechanical properties of rock material under the combined effects of high temperature and pressure have been an important and challenging issue for decades. The research of thermal properties of rocks at high temperature or after heat treatment can provide valuable information for the development and solution of applied problems in geothermal engineering, such as rock drilling, ore crushing, deep mining under high temperature and high ground pressure [1], geothermal energy extraction [2], high-level nuclear waste disposal [3], [4] and the protection of buildings against fire or building restoration after exposure to fire [5].

Investigations of the physical and mechanical properties of rocks have been performed by several researchers when rock engineering is subject to paroxysmal high temperature. Wu *et al.* [6] studied the changes of shape, volume, mass and den-

sity and the velocity variations of longitudinal and transverse elastic waves through the samples before and after exposure to high temperature. Besides, also included are the mechanical properties of the stress–strain response, the uniaxial compressive strength, the modulus of elasticity and the Poisson's ratio. Homand-Etienne and Houpert [7] analyzed the mechanical behavior of thermally induced micro-cracking in granites. Mambou *et al.* [8] investigated the effect of ISO 834 fires on the mechanical properties of a granite specimen submitted to uniaxial loading, and established the rate-equation model of the granite rock specimen under mechanical load and fire based on Newton's second law. The thermal effect on the mechanical performance of granite at the center and the ends of the specimen were also analyzed. Shabbir *et al.* [9] measured the thermal conductivity and thermal diffusivity of marbles between 290 and 335 K in dry air at atmospheric pressure, which showed a slight increase in thermal conductivity with temperature. Rocchi *et al.* [10] studied the mechanical properties of volcanic rocks at high temperatures and low pressures, and showed that the Vesuvian and Etnean rocks remain fully brittle up to 600 °C with typical strengths of 90 MPa and 100 MPa and Young's modulus of 60 GPa and 40 GPa, respectively. Above this temperature, the elastic modulus and compressive strength decrease steadily in both the Vesuvian and Etnean rocks, reaching 10% of the original values at 900°C and 800°C, respectively, when partial melting occurred. Yavuz *et al.* [11] investigated the effect of thermal damage on the physical properties of five carbonate rocks (two marbles and three limestones), and found that compaction of the rock structure up to 150 °C occurred and that the induced calcite dilation had no significant damage effect on the rock material. However, compaction of the rock structure led to an increase in the P-wave velocity and a slight decrease in porosity. Lindholm *et al.* [12] performed many tests involving uniaxial compression or extension with different confining pressures, strain rates and temperatures, and the relationship between the rock strength, temperature, and the strain rate was established.

With further research on the mechanical properties of the rock and the rapid development of dynamic loading equipment, the focus of scholars is not limited to the static conditions, and more and more people are turning their attention to the dynamic properties of rock [13], [14]. Since Li *et al.* [15] put forward a shaping technology by using a special-shaped striker, the half-sine wave loading technology was quickly accepted and promoted by academic circles, as it provides better stability of the strain rate and more representative results than those obtained from the conventional rectangular loading waveform shape. Frew *et al.* [16] conducted modified uniaxial compressive SHPB tests on limestone by placing a thin copper disk on the impact surface of the incident bar as a pulse shaper, which showed the dynamic stress equilibrium of samples and had constant strain rates over most of the test durations. SHPB experimental technology as an effective means of dynamic mechanical properties testing has been greatly developed and applied. Therefore, the dynamic testing of rock under the coupled effect of temperature and pressure can be carried out smoothly.

The thermal damage constitutive model can well reflect the damage and failure process and stress–strain relationship of rock, which is one of the key problems in rock mechanics [17], [18]. Based on hundreds of groups of rock triaxial test data and a large number of geotechnical field test results of statistical analysis, and combined with the rock traits from the theoretical research results and practical tests, Hoek and Brown [19] established the Hoek–Brown criterion in 1980s. Over the years, with continued development and perfection by a large number of scholars, it has been revised and can be used to derive the constitutive model of rock damage, achieving good results [20], [21]. In addition, Liu *et al.* [22] built a new damage constitutive model based on energy dissipation, developed to describe the behavior of rocks under cyclic loading. The results showed that the values of the damage variables increase exponentially with strain. The amended damage constitutive model can describe the degree of compactness of rocks accurately, and the damage constitutive model under cyclic loading has reasonable error in describing the behavior of rocks under cyclic loading. Wen-Gui *et al.* [23] established a statistical damage constitutive model for strain-softening of rock based on normal distribution, which can reflect the effect of different confining pressures.

This study conducted a series of laboratory tests with the split Hopkinson bar system to examine the physical and mechanical properties of thermally treated Changsha sandstone specimens under uniaxial dynamic loading. The changes of longitudinal wave velocity and the influence of dynamic strength and microcosmic mechanism on the mechanical properties of the sandstone under the impact load are analyzed. Furthermore, according to generalized Hooke's law and strain equivalence assumption, any strain constitutive relation of damaged material can be derived from the constitutive equation of lossless material. The damage constitutive relation of the rock was established by introducing the statistical theory, and the rock microstructural strength was described by the axial strain from the randomness of the internal flaws distribution of the rock material [24], [25], [26]. Some parameters and curves that can reflect the rock deformation and failure process were presented, so as to establish the damage constitutive model to describe the path of the rock damage, and its macroscopic manifestation and the whole process from deformation to damage are verified by the test results.

II. SAMPLE PREPARATION AND EXPERIMENTAL METHODOLOGY

A. SAMPLING AND HIGH TEMPERATURE TREATMENT

The rock material used in this study was medium-strength sandstone that is widely available in the Changsha area of Hunan province, China. Microscopic studies in the form of optical microscopy and X-ray diffraction were performed

TABLE 1. Physical and mechanical properties of sandstone at normal temperature (25°C).

Specimen	Density (g/cm^3)	P-wave Velocity (m/s)	Compressive Strength (MPa)	Young's Modulus(GPa)	Poisson's Ratio	Friction Angle(°)
Sandstone	2.68	3218	126.8	27.07	0.29	43

to provide an insight into rock mineralogical composition and grain sizes, as showed in Fig. 1 and 2. According to these analyses the sandstone under study is mainly composed of quartz 65.68%, feldspar 21.35%, montmorillonite 4.58%, mica 3.67% and chlorite 4.72%. According to the requirements of the rock dynamic mechanical testing procedures suggested by the ISRM [27], [28], cylindrical sandstone specimens with 50mm in diameter and 30mm in length were polished to ensure that the two end planes of the sample were parallel with an accuracy of ±0.05mm and the surface roughness was within 0.02mm. Some fundamental parameters of the tested sandstone at room temperature are listed in Table 1.

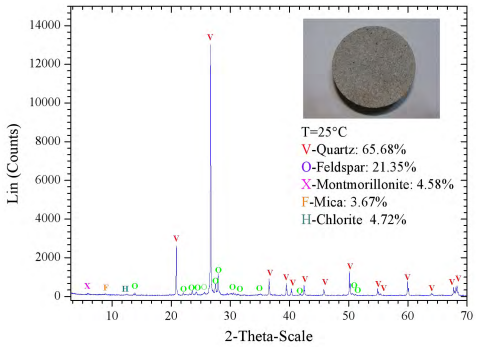

FIGURE 1. XRD analysis of the Changsha sandstone at room temperature.

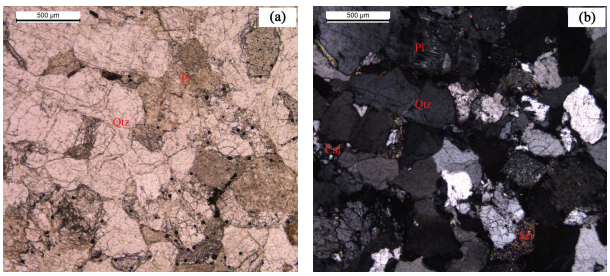

FIGURE 2. Petrographic microscopy images of the Changsha sandstone under (a) PPL and (b) XPL (Qtz-quartz; Pl-plagioclase; Cal-calcite; Ser-Sericite).

In this study, all sandstone samples were treated with the same heat treatment method, including three stages of heating, heat preservation and cooling. Twenty samples were divided into five groups were prepared for this study: four groups were heat-treated at 200, 400, 600 and 800°C, respectively, while the remaining one group remained untreated at room temperature (25°C). The heat treatment was carried out in an electrical furnace SX-4-10, composed of a temperature controller and heating furnace, showed in Fig. 3 (a). The maximum operating temperature of the device is 1050°C,

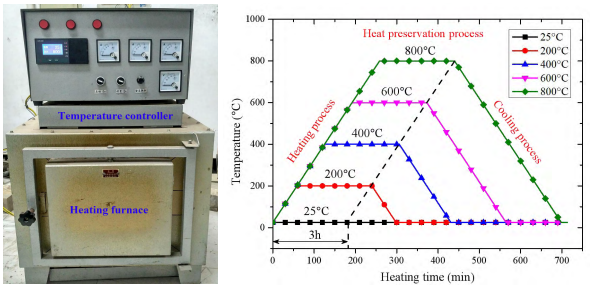

FIGURE 3. Rock heat treatment equipment and temperature variations with heating time. (a) High temperature equipment. (b) Heating process.

with programmable controller to control the temperature and heating rate. Fig. 3 (b) gives the temperature variations of rock with heating time, and there are two key technologies during the process of rock heat treatment. The first is to adopt a lower heating and cooling rate (3°C/min) to avoid thermal shock damage of rock [29], [30]. The other is that the specimens were kept at each predetermined temperature for 3 hours, which purpose is to make sure that the rock is heated uniformly from outside to inside, with no temperature gradient [31], [32].

B. STRESS-STRAIN CURVES UNDER STATIC COMPRESSION

Prior to the dynamic compressive tests, initial sandstone damage characteristics caused by heat treatment were studied, with static loading tests performed using an MTS hydraulic servo-control testing machine. A constant loading rate of 200N/s was selected for all tests following the method suggested by the ISRM [27]. The resulting stress–strain curves of sandstone specimens treated under the five different temperatures are showed in Fig. 4.

It could be observed that the typical stress-strain curves at each temperature are basically divided into four stages: compaction, elasticity, yield and failure. The static compressive strength of sandstone decreases continuously with the increase of treatment temperature. The deformation of sandstone increases with the increase of treatment temperature, and the compaction stage increases with the increase of temperature. All these above phenomena indicate that high temperature causes damage to rocks. Another problem that needs to be noticed is that the total stress-strain curve is obviously disorderly after 400 °C, which is due to the large changes in the internal structure of the rock after the high temperature treatment, and the growth of the primary cracks.

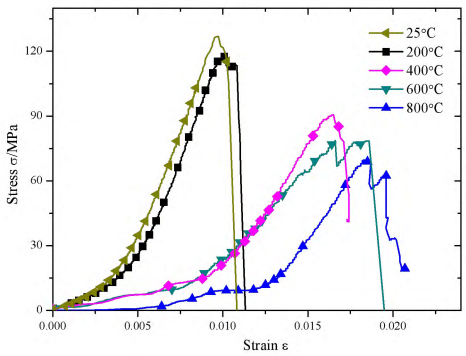

FIGURE 4. Axial stress-strain curves of sandstone under static compression with different heat-treatment temperature.

C. TESTING APPARATUS AND PROCEDURE

The traditional SHPB system consists of a striker, an incident bar, a transmission bar, an absorption bar and other auxiliary components like a gas gun and a data recording unit [33], shown in Fig. 5. The sample was sandwiched between the incident and transmission bars. The lengths of the striker bar, incident bar, transmission bar and absorption bar are 360.1 mm, 2000 mm, 1500 mm and 500 mm, respectively. All of these elastic bars were made of 40Cr alloy steel with high yield strength. Two semi-conductor strain gauges were attached on the incident and transmission bars to record the signals from the sample. A 16-channel Yokogawa digital oscilloscope was used to record strain gauge signals collected from the bridge circuits after amplification. And a high-speed camera was used to record the rock failure process. Based on the one-dimensional stress wave theory, ε represents the measured signals on the bars, while the incident wave, reflected wave and transmitted wave are denoted with subscripts I, R and T, respectively. According to one-dimensional wave theory, the stress, strain and strain rate of the sample can be expressed as [34]:

$$\sigma(t) = \frac{A_e E_e}{2A_s}[\varepsilon_I(t) + \varepsilon_R(t) + \varepsilon_T(t)] \tag{1}$$

$$\varepsilon(t) = \frac{C_e}{L_s}\int_0^t [\varepsilon_I(t) - \varepsilon_R(t) - \varepsilon_T(t)]dt \tag{2}$$

$$\dot{\varepsilon}(t) = \frac{C_e}{L_s}[\varepsilon_I(t) - \varepsilon_R(t) - \varepsilon_T(t)] \tag{3}$$

where A_e, C_e and E_e are respectively the cross-section areas, wave velocity and Young's modulus of elastic bars. A_s and L_s are the cross-sectional area and the length of the sample.

D. SPECIAL-SHAPED STRIKER FOR SHPB

For some brittle materials, it is difficult to reach dynamic stress equilibrium because the specimen may produce failure immediately before several reflections of the wave when it is impacted. In some practices like drilling, forging, stamping and piling, different impacting tools will produce different waveforms. This indicates that the waveform has a relation with the striker geometry. For this work, in earlier studies, Li *et al.* [35] and Zhou *et al.* [36] designed various strikers, which produce different shapes of stress waves, to carry out the impact test with rock breakage as the target. Collation of the information on the dynamic constitutive relation of rock under different loading waves makes it clear that the dynamic constitutive relation of rock must be used to load a half-cycle sine wave. Zhu *et al.* [37] established the stress wave inversion theory of an arbitrary cross-section striker hitting the long rod, and developed the ideal load wave corresponding to the striker structure, which solves the inherent defects of the traditional loading method. In the SHPB test, the spindle-shaped striker loading style changes the loading waveform while changing the loading conditions at the end of the bar. If the incident bar is too short, it cannot guarantee that the specimen will be under uniform loading. And when the elastic wave propagates in the elongated bar, the wave will diffuse due to the lateral inertia effect. To this end, our team used a numerical simulation to study the propagation and stress distribution of the stress wave in the elastic wave under loading waves of different waveforms and different spatial distributions.

We obtained the stress wave evolution and cross-sectional stress uniformity of the general rules, so as to guide the design and selection of the shape of the striker and the length of the elastic rod for the SHPB experiment. Fig.6 shows the simplified special-shaped striker geometries fabricated in the SHPB with a diameter of 50 mm to produce half-sine waves. In practice, the microscopic particle size of the rock is usually 2∼5 mm, while the sample diameter should be in the range of 20∼50 mm, so the 50 mm diameter of the transmission rod is suitable for most rocks. The other parameters of the rod are: elastic modulus 240 GPa, density 7800 kg·m-3, Poisson's ratio 0.285. The strain gauges were pasted 733 and 655 mm away from the bar–sample interfaces on the incident bar and transmission bar, respectively. Fig. 7 shows typical stress histories at both ends of the sample of a rectangular wave with

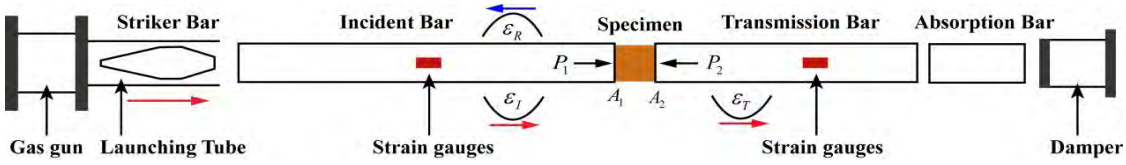

FIGURE 5. Schematic of a split Hopkinson pressure bar (SHPB) system.

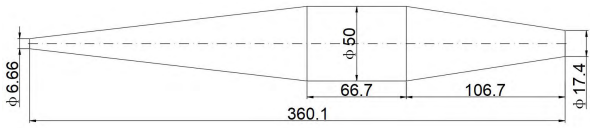

FIGURE 6. Schematic of a spindle-shaped striker.

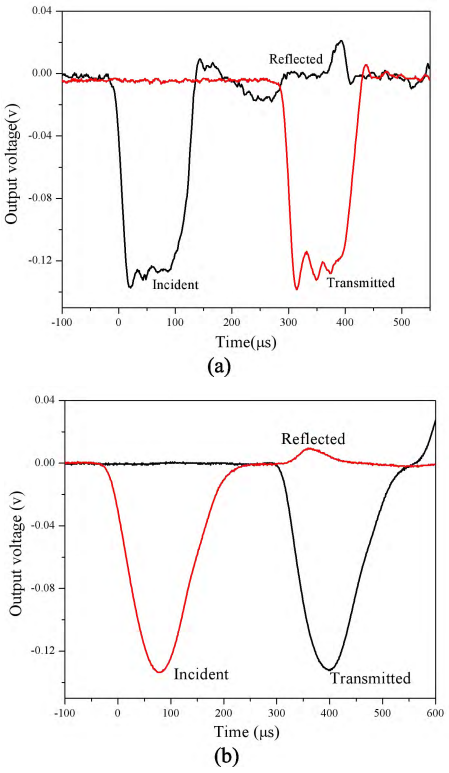

FIGURE 7. Rectangular and half-sine waveforms.

the traditional cylindrical striker and an improved half-sine wave with the special-shaped striker technique. The results indicated that the rising section of the half-sine wave produced by the special-shaped striker is obviously reduced, and in particular the waveform oscillation is no longer apparent.

III. EXPERIMENTAL RESULTS

A. STRESS EQUILIBRIUM VERIFICATION

For any valid SHPB experiment, it is a prerequisite that, during the test, the force across the sample should be approximately the same [38]. In this study, a cone-shaped striker was utilized as a pulse-shaping device, as employed successfully elsewhere [39], [40]. The loading forces on both ends of the sample are obtained via the following formula:

$$P_1 = EA\left[\varepsilon_I(t) + \varepsilon_R(t)\right] \tag{4}$$

$$P_2 = EA\varepsilon_T(t) \tag{5}$$

Where E and A are the elastic modulus and the cross-sectional area of the bar, respectively; and ε_I, ε_R and ε_T respectively represent the incident, reflection and transmission strain of the bar.It can be observed from Fig. 8 that

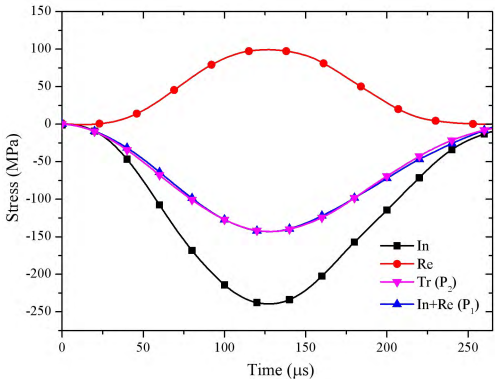

FIGURE 8. Dynamic stresses on both ends of specimen tested using a modified SHPB with a spindle-shaped striker. In, Re, Tr denote incident, reflected, and transmitted wave, respectively.

the dynamic forces on both sides of the specimen are in a state of balance, as the sum of the incident (In) and reflected (Re) stress waves is absolutely equal to the dynamic force transmitted on the other side, and the axial inertial effect can be neglected in the dynamic tests.

B. DYNAMIC STRESS-STRAIN RELATIONS

Fig.9 shows the dynamic compression stress–strain results of sandstone after different high temperature treatments. It can

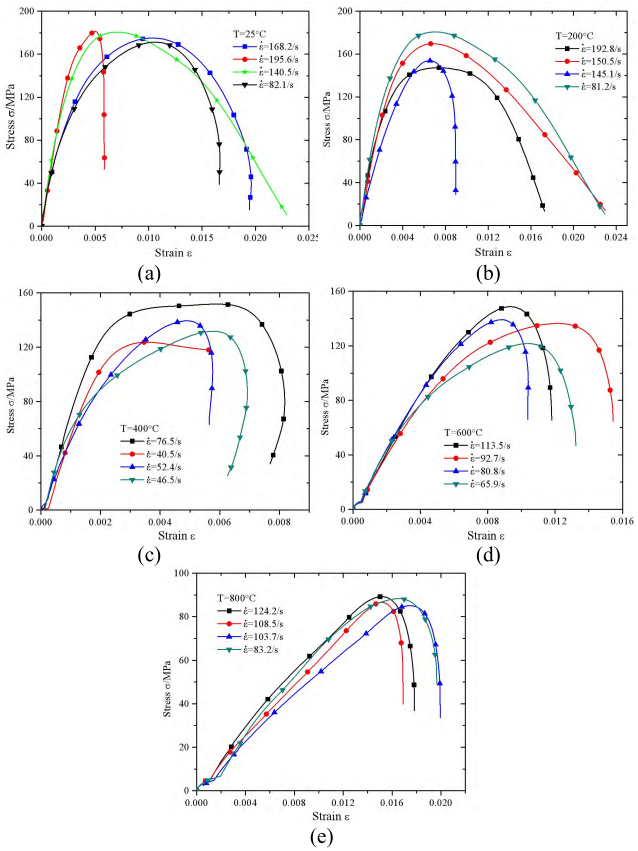

FIGURE 9. Dynamic stress-strain curves of sandstone for different heat-treatment temperature.

be observed from Fig.9 (a) and (b) that the dynamic compressive stress–strain curves of the sandstone emerged into three stages, elasticity, yield and failure before the temperature of 200°C. There is no compaction stage compared with the static tests, directly into the elastic phase, the stress and strain curve appeared to have a linear proportional relationship. The elastic modulus is larger than the static (this can be clearly seen from the slope of the stress–strain curve), which is probably because there is not enough time for internal microcracks to close, and the internal crystals show a large inertial force under the high-speed impact loading. In the yield stage, the stress–strain curve deviates from the straight line. This is perhaps because the lower strength materials inside the rock were first destroyed and produced new cracks, while the surrounding materials were gradually destroyed by being subjected to high stress, so that fissures continued to evolve. Finally, due to the internal cracks growth and coalescence, macro-damage formed and the whole sample reached the ultimate bearing capacity and entered the failure stage.

Fig.9 (c)∼(e) shows the stress–strain relationship variation of the sandstone after 400∼800 °C high temperature heat treatment and cooling down to normal temperature. It can be seen from the figure that after high temperature treatments, the slope of the dynamic stress–strain curve (the elastic modulus) decreases, and the strain magnitude changes greatly with the increase of the temperature. This can be explained by the following reasons: (1) Due to the different thermal expansion rate of the rock minerals being exposed to high temperatures, strains are gradually accumulated in crystal particles, and some defects and fractures will occur when the rocks cool down. (2) After being heated at 400∼800 °C, thermal cracks occurred in crystal particles inside the rock, the higher the temperature, the greater the degree of thermal cracking, and after cooling the rock could not restore the original state of the cracks formed. (3) When the temperature ranges from 400 to 800 °C, some complex changes occur, such as mineral component decomposition, constitution water evaporation and phase transition due to the combined action of melting and structural thermal stress. The internal porosity of the rock caused by these factors increases, and the elastic modulus decreases under the impact load. It should be noted that sandstone specimens that have been heat treated above 400°C also exhibit compaction under dynamic compression conditions, and the higher the preheating temperature, the more pronounced the compaction stage. This may be due to the appearance of a lot of larger pores in the specimen after the high temperature effect. The rock structure is no longer compact and the effect of strain rate under dynamic loading is weakened. Under the impact load, the closed process of the pores cannot be neglected and the compaction phase will be reappeared.

C. COMPRESSIVE STRENGTH VARIATION WITH TEMPERATURE

Fig. 10 presents the relationship of the dynamic compressive strength with the treatment temperatures of the sandstone,

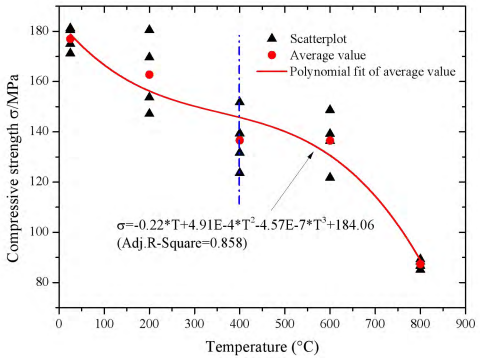

FIGURE 10. The variation of dynamic compressive strength with temperature.

indicating that, despite the largely discrete test results, there still exists a clear general trend whereby the compressive strength decrease obviously with the increase of temperature. At the temperature of 25 to 400 °C, the value of the strength decreased from 177.0MPa to 136.6MPa, the reduction rate reached 22.8%. This can be explained by the increase in both the number and width of the thermally induced micro-cracks with the heating temperature: below 200 °C, the crystal water inside the rock evaporates out and creates a lot of voids, while at 200∼400°C due to the deformation occurring in the internal mineral particles and the structural thermal stress caused by different minerals in the composition of the ore at high temperature, some micro-cracks gradually develop into larger cracks after cooling down, which causes the dynamic strength to decrease.

When the temperature exceeds 400 °C, the dynamic strength decreases faster again, perhaps because the quartz within the sandstone undergoes α-β phase transformation at 573°C, which leads to an increase in cracks, and some fused, easily decomposed, and easily evaporated. The role of minerals made that small cracks develop into large cracks caused by a sharp decline in strength. After being treated at 800°C, the average peak strength decreased to 87.4 MPa, this decrease rate being as high as 50.6% compared with the room temperature.

IV. THERMAL-MECHANICAL COUPLING CONSTITUTIVE MODEL

The dynamic constitutive model of rock is the basic parameter to analyze the effect of rock structure on dynamic load, and it acts as a liaison between theory and application. In order to improve the application scope of this model, this paper established a dynamic uniaxial constitutive model, using the experimental results to verify it.

A. P-WAVE VELOCITY AND THERMAL DAMAGE OF ROCK

Under the action of temperature load, thermal stress is generated inside the rock, producing a large number of microcracks and gradually expanding through, leading to the degradation of the mechanical properties. This progressive failure

of the rock caused by the accumulation of micro-cracks can be represented by thermal damage D_T. According to the theory of macroscopic damage mechanics, the thermal damage D_T can be represented by the change of rock mechanical parameters, which is defined as [41]:

$$D_T = 1 - \frac{V_T^2}{V_0^2} \tag{6}$$

Where D_T is the thermal damage variable, representing the degree of thermal damage. V_T, V_0 represent the P-wave velocity after the temperature T and 25 °C, respectively. It follows from this definition that the value of the scale variable D_T (which depends upon the point and the direction considered) is bounded by 0 and 1, that is, $0 \leq D_T \leq 1$. $D = 0$ indicates that no damage occurred, and $D_T = 1$ is fully broken into more than two parts. In fact, the failure occurs for $D_T < 1$ through a process of instability.

Figure 11 shows the variation of ultrasonic P-wave velocity with treatment temperature. It could be observed that the longitudinal wave velocity of sandstone after cooling is reduced to varying degrees with the increase of temperature. And the decrease rate increases with the increase of temperature. When the temperature is blow 200 °C, the longitudinal wave velocity shows a slow decrease than the normal temperature. When the temperature exceeds 200°C, the longitudinal wave velocity decreases linearly, with a greater decrease rate. After 800°C high temperature, the average wave velocity of sandstone decreased from 3227m/s at room temperature to 1189m/s, and the reduction rate reached 63%. The main reason causing the decrease of P-wave velocity is due to the difference of the coefficient of mineral expansion in the rock, which leads to the expansion of the crack and the emergence of the new fissure. On the other hand, under the action of high temperature, the water inside the pore of rock is evaporated which resulted the volume of pore increases. The pore has a barrier effect on the propagation of wave velocity, resulting in the increase of wave energy attenuation and the decrease of wave velocity.

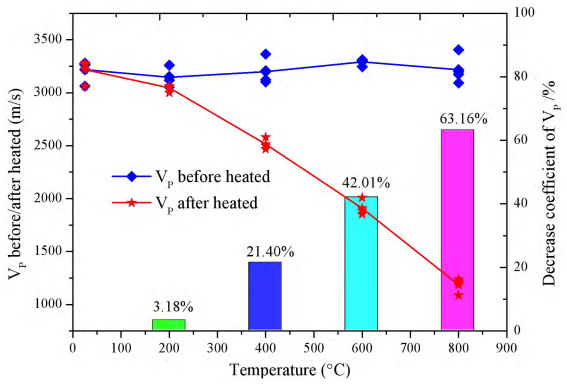

FIGURE 11. Variation of ultrasonic P-wave velocity with treatment temperature.

According to the calculation method of thermal damage in formula 6, it could be observed that the thermal damage keep a three stages increase with the increase of treatment temperature, showed in Fig. 12.

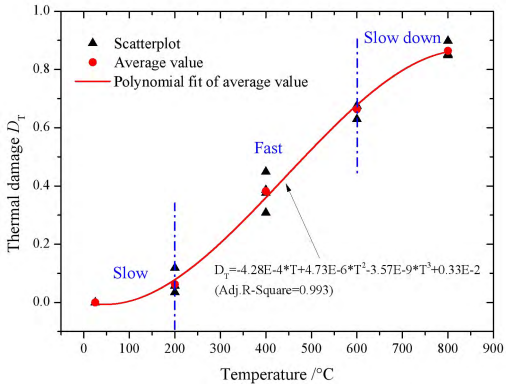

FIGURE 12. The variation of thermal damage with temperature.

At the temperature range from 25 to 200°C, due to the evaporation of free water inside the rock, pores and micro defects between some mineral particles were exposed. But owing to the expansion of mineral particles, some original and newly exposed fissures will be tightly compacted, which resulted the thermal damage of rock shows a slow increase. Within the temperature range of 200 to 600°C, strongly bound water and constitution water gradually escaped, especially, when temperature rises to 573 °C, the α-β quartz phase transition will be occurred [42], which resulted in the internal structure of rock is no longer dense and the thermal damage of rock increases rapidly. However, when temperature exceeds 600°C, the internal structure of the rock has been very loose, although the high temperature action will still lead to cracking initiation and expansion, but the increase rate will be slow during this stage.

B. DYNAMIC STATISTICAL DAMAGE CONSTITUTIVE MODEL

The micro-cracks, voids, and internal defects are the main factors that lead to rock damage, and because of the random distribution of flaws such as cracks and voids in the rock material, its strength value is not the same, so it is obvious that describing the mechanical properties of the constituent components with a single eigenvalue of the intensity value is impossible [43], [44]. Since Krajcinovic *et al.* [24] proposed their statistical damage model, it has been greatly developed, and in rock materials the Weibull damage distribution method is widely used. Based on previous studies, the Weibull distribution is used in this paper, which is expressed as:

$$\varphi(F) = \frac{n}{F_0}\left(\frac{F}{F_0}\right)^{n-1} \exp\left[-\left(\frac{F}{F_0}\right)^n\right] \tag{7}$$

where $\varphi(F)$ stands for the mesoscopic element strength distribution function, F is the random variable of the Weibull distribution, F_0 and n are the Weibull statistical distribution parameters.

In this method, assuming that the rock is composed of a large number of micro-elements, the micro-body size is large enough to contain a large number of micro-defects, while in the mechanics sense, it is small enough to be regarded as a particle. Figure 13(a) gives a time-dependent damage model considering thermal damage, which is a combination of the damage body and the viscous body in any plane of space. Viscous material has no damage characteristics, and under static loading the viscous body does not play a role but becomes a transparent body, whereas, when the loading rate reaches a certain value, the viscous body will play an effective role. The constitutive relationship of the viscous body is as follows:

$$\sigma = \eta \frac{d\varepsilon}{dt} \tag{8}$$

where η is the viscosity coefficient, reflecting the viscous properties of rock or stone, which can be determined by the rock creep test, with the general viscosity coefficient of the rock ranging from 0.1 to 0.5.

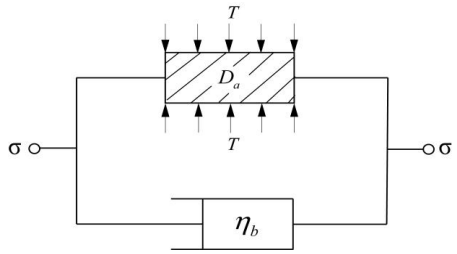

(a)

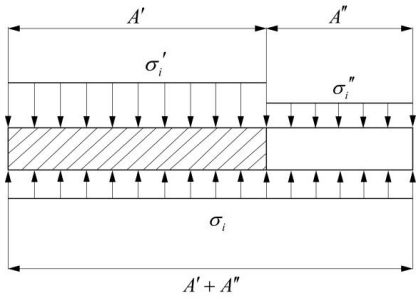

(b)

FIGURE 13. The damage model for rock considering initial voids. (a) Time-dependent damage model considering thermal damage; (b) Microstructure of rock damage.

Based on the assumption that the micro-body strength obeys the statistical distribution, the degree of damage to the rock can be measured by the ratio of the number of destroyed elements to the total number of elements. Assuming that the number of the cumulative damage is N_f, the total number of micro-elements is N, and the damage state of the rock can be expressed as:

$$D_M = \frac{N_f}{N} \tag{9}$$

where D_M is the mechanical damage variable, representing the degree of damage caused by stress. According to this definition method, the value of the scale variable D_M is bounded by 0 and 1, that is, $0 \le D_M \le 1$. $D_M = 0$ indicates that no damage occurred, and $D_M = 1$ means fully broken, almost losing the loading capacity.

Thus, when the stress level is F the number of damaged micro-elements in the rock is N_f, and we can obtain:

$$N_f = \int_0^F N\varphi(F)dF \tag{10}$$

The mechanical damage D_M is the description of the accumulated effect of the element destruction during rock loading, where the relationship between D_M and $\varphi(F)$ can be defined as:

$$D_M = \left(N\int_0^F \varphi(F)dF\right)\Big/N = 1 - \exp\left[-\left(\frac{F}{F_0}\right)^n\right] \tag{11}$$

In 1952, Drucker and Prager proposed the Drucker–Prager yield and failure criterion for rock and soil materials, which can be considered as the generalized von Mises criterion. Lemaitre [41] applied it to the study of damage mechanics, and the expression is:

$$F = f(\sigma^*) = \alpha_0 I_1^* + \sqrt{J_2^*} \tag{12}$$

where α_0 is the constant which is related to the internal friction angle of rock material, I_1^* is the first effective stress invariant, J_2^* is the second effective biased stress invariant. These are represented as:

$$\alpha_0 = \sin\varphi \Big/ \sqrt{9 + 3\sin\varphi} \tag{13}$$

$$I_1^* = \sigma_1^* + \sigma_2^* + \sigma_3^* = \frac{E\varepsilon_1(\sigma_1 + \sigma_2 + \sigma_3)}{\sigma_1 - \mu(\sigma_2 + \sigma_3)} \tag{14}$$

$$J_2^* = \frac{1}{6}\left[(\sigma_1^* - \sigma_2^*)^2 + (\sigma_2^* - \sigma_3^*)^2 + (\sigma_1^* - \sigma_3^*)^2\right] = \frac{E^2\varepsilon_1^2\left(\sigma_1^2 + \sigma_2^2 + \sigma_3^2 - \sigma_1\sigma_2 - \sigma_2\sigma_3 - \sigma_1\sigma_3\right)}{3\left[\sigma_1 - \mu(\sigma_2 + \sigma_3)\right]^2} \tag{15}$$

where σ_1 is the maximum principal stress (MPa); σ_3 is the minimum principal stress (MPa); φ is the internal friction angle of the rock material.

Considering it in the one-dimensional case, where there is $\sigma_2 = \sigma_3 = 0$, $\varepsilon_1 = \varepsilon$, the micro-body strength expressed by the effective stress invariant is as follows:

$$F = \left(\alpha_0 + \frac{1}{\sqrt{3}}\right)E\varepsilon \tag{16}$$

As shown in Fig. 13(a), assuming that the impulse load applied in the horizontal direction of the micro-element is σ, the stress–strain of the micro-element model should satisfy the following relationship:

$$\begin{cases} \varepsilon = \varepsilon_a = \varepsilon_b \\ \sigma = \sigma_a + \sigma_b \end{cases} \tag{17}$$

According to the strain equivalence hypothesis presented by Lemaitre [45], the strain produced by a damaged material under effective stress is equivalent to the strain that occurs when the same material is lossless. The basic structure of the micro-element model is shown in Fig. 13(b). It is assumed that the rock produced under stress is composed of two parts, that is, the undamaged material and the damage material. The total load of rock materials is shared by these two parts. Under a uniaxial stress state, any strain constitutive equation established for damage can be used to derive the same equation for the lossless material, except that the usual stress needs to be replaced by an effective stress:

$$\sigma^* = \frac{\sigma}{1 - D_M} \tag{18}$$

where σ^* is the effective stress or actual stress, σ is the general stress. Combined with the Hooke's law for linear elasticity, the strain can be expressed as:

$$\varepsilon = \frac{\sigma^*}{E} = \frac{\sigma}{E(1 - D_M)} \tag{19}$$

Substituting Equation (11) into Equation (19), the stress–strain relationship is obtained as:

$$\sigma = E\varepsilon(1 - D_M) = E\varepsilon \exp\left[-\left(\frac{F}{F_0}\right)^n\right] \tag{20}$$

When the constitutive relation of the damaged body and the viscous body is substituted into Formula (17), the statistical damage constitutive equation of rock under the one-dimensional stress state is obtained as:

$$\sigma = E\varepsilon \exp\left[-\left(\frac{\left(\alpha_0 + \frac{1}{\sqrt{3}}\right)E\varepsilon}{F_0}\right)^n\right] + \eta.\frac{d\varepsilon}{dt} \tag{21}$$

There are two Weibull distribution parameters (F_0 and n) in the above constitutive model that have not been determined. In the rock stress–strain curve, when the axial stress reaches its peak value, the peak stress σ_f and the corresponding strain ε_f satisfy the following geometrical conditions:

$$\varepsilon = \varepsilon_f, \quad \sigma = \sigma_f \tag{22}$$

$$\varepsilon = \varepsilon_f, \quad \frac{d\sigma}{d\varepsilon} = 0 \tag{23}$$

where $\frac{d\sigma}{d\varepsilon}$ is:

$$\frac{d\sigma}{d\varepsilon} = E\left[1 - n\left(\frac{\left(\alpha_0 + 1/\sqrt{3}\right)E\varepsilon}{F_0}\right)^n\right] \times \exp\left[-\left(\frac{\left(\alpha_0 + 1/\sqrt{3}\right)E\varepsilon}{F_0}\right)^n\right] \tag{24}$$

According to the peak point on the stress–strain curve $(\sigma_f, \varepsilon_f)$, the test strain rate $\frac{d\varepsilon}{dt}$ and the rock material constant E, η, φ can directly determine the damage model parameters m and F_0.

Combining Equations (22), (23) and (24) with Equation (21), the expression of n is:

$$n = \frac{1}{\ln(E\varepsilon_f) - \ln(\sigma_f - \eta\frac{d\varepsilon}{dt})} \tag{25}$$

The relation of F_0 and n is expressed as:

$$F_0 = \left(\alpha_0 + 1/\sqrt{3}\right)E\varepsilon_f n^{\frac{1}{n}} \tag{26}$$

Substituting Equations (25) and (26) into Equation (11), the D_M is obtained as:

$$\begin{aligned} D_M &= 1 - \exp\left[-\left(\frac{F}{F_0}\right)^n\right] \\ &= 1 - \exp\left\{-\left[\ln(E\varepsilon_f) - \ln(\sigma_f - \eta\frac{d\varepsilon}{dt})\right] \times \left(\frac{\varepsilon}{\varepsilon_f}\right)^{\frac{1}{\ln(E\varepsilon_f) - \ln(\sigma_f - \eta\frac{d\varepsilon}{dt})}}\right\} \end{aligned} \tag{27}$$

C. THERMAL-MECHANICAL COUPLING DAMAGE

The definition of the rock damage value has always been a very troublesome problem, especially in the case of a variety of load couplings, usually based on the ideal state under the assumption that is used to guide the application of rock damage mechanics in practice.

Under the action of temperature and load, the rocks show different damage characteristics. High temperature will cause the evaporation of free water inside the rock, the expansion of fractures and even the transformation of mineral composition, which will lead to the deterioration of the mechanical properties of rock. Under high strain rate loading, rock exhibits obvious strain rate hardening effect. The total damage of the loaded rock under high temperature conditions can be measured by the generalized damage variables derived from the equivalent strain principle, where the total damage D equals [46]:

$$D = D_T + D_M - D_T D_M \tag{28}$$

By substituting Equations (6) and (27) into Equation (28), the total thermo-mechanical coupling damage is:

$$D = 1 - \frac{V_T^2}{V_0^2}\exp\left\{-\left[\ln(E\varepsilon_f) - \ln(\sigma_f - \eta\frac{d\varepsilon}{dt})\right] \times \left(\frac{\varepsilon}{\varepsilon_f}\right)^{\frac{1}{\ln(E\varepsilon_f) - \ln(\sigma_f - \eta\frac{d\varepsilon}{dt})}}\right\} \tag{29}$$

The process of rock deformation and failure is actually the process of internal crack initiation, compaction, expansion, convergence and penetration. Under the condition that the stress value is lower than the initiation stress, the crack inside the rock does not expand and the rock is not damaged. Therefore we can suppose that there is a threshold point in the rock deformation process: when the rock stress state is less than the threshold, there is no mechanical damage evolution or the value is very small or zero and the total damage to the rock is preheating damage; when the stress state is larger than

the initiation stress, the damage can be expressed by (29). It should be noted that under the mechanical loading, some of the vulnerable elements inside the rock will be destroyed, and this will cause some damage to the rock in the macro-performance. When the stress is small at room temperature, the macroscopic damage to the rock is very small or zero, so many scholars propose that the rock will experience a basic negligible damage. But after high temperature, as the rock at the same stress level, it will not produce damage or the damage will be less than at the normal temperature state. Since we know, rock material is not an ideal elastomer, when the stress is large, it will cause damage to the rock and the damage will accumulate. From the energy point, part of the energy accumulate in elasticity body, the other part of the energy cause rock damage, which also explains why rock burst does not occur after rock stress over its elastic limit.

Deriving Equation (29) with respect to ε, the equation of the damage evolution rate of the rock is obtained as:

$$\frac{dD}{d\varepsilon} = \frac{V_T^2}{\varepsilon_f V_0^2} \exp\left\{-\left[\ln(E\varepsilon_f) - \ln(\sigma_f - \eta\frac{d\varepsilon}{dt})\right] \times \left(\frac{\varepsilon}{\varepsilon_f}\right)^{\frac{1}{\ln(E\varepsilon_f)-\ln(\sigma_f-\eta\frac{d\varepsilon}{dt})}}\right\} \cdot \left(\frac{\varepsilon}{\varepsilon_f}\right)^{\frac{\ln\left(\sigma_f-\eta\frac{d\varepsilon}{dt}\right)-\ln\left(E\varepsilon_f\right)+1}{\ln(E\varepsilon_f)-\ln(\sigma_f-\eta\frac{d\varepsilon}{dt})}} \tag{30}$$

When the unknown parameters are connected into the model, the stress–strain relationship can be expressed as:

$$\begin{aligned}\sigma &= E\varepsilon(1-D_M)\\ &= E\varepsilon \exp\left\{-\left[\ln(E\varepsilon_f) - \ln(\sigma_f - \eta\frac{d\varepsilon}{dt})\right] \times \left(\frac{\varepsilon}{\varepsilon_f}\right)^{\frac{1}{\ln(E\varepsilon_f)-\ln(\sigma_f-\eta\frac{d\varepsilon}{dt})}}\right\} + \eta\frac{d\varepsilon}{dt}\end{aligned} \tag{31}$$

Based on the extended equivalence principle of the proposal by Zhang *et al.* [47], we can regard the preheat damage as a baseline damage. Through the study, we found that E_T is approximately equal to $E_0\,(1-D_T)$, if it is used only to make a rough estimate of the compressive strength of the rock, and Equation (31) can be rewritten as:

$$\begin{aligned}\sigma &= E_0\varepsilon(1-D)\\ &= E_0\varepsilon\frac{V_T^2}{V_0^2} \exp\left\{-\left[\ln(\frac{E_0V_T^2\varepsilon_f}{V_0^2}) - \ln(\sigma_f - \eta\frac{d\varepsilon}{dt})\right] \times \left(\frac{\varepsilon}{\varepsilon_f}\right)^{\frac{1}{\ln(E\varepsilon_f)-\ln(\sigma_f-\eta\frac{d\varepsilon}{dt})}}\right\} + \eta\frac{d\varepsilon}{dt}\end{aligned} \tag{32}$$

where E_0 is the elastic modulus at room temperature.

D. MODEL VALIDATION AND PHYSICAL MEANING OF PARAMETERS

The determination of the model parameters n and F_0 is one of the key problem to establish the statistical model of rock damage statistics, it can use the experimental data of this paper to determine. The parameters internal friction angle φ and viscosity coefficient η need to be determined by rock shear test and creep test respectively. This paper limited to the experimental conditions and there is no measured test data. However, it can be seen from the calculation of the model parameters that the internal friction angle φ and viscosity coefficient η have little effect on the fitting results of the model. According to the Mohr–Coulomb strength theory, the actual factors influencing and restricting the rock strength are the internal friction angle and the cohesive force. The melting and disappearing of fusible materials in the rock lead to the growth of micro-fissures under high temperature, while the effect of temperature rise on the microstructure of the specimen is weak, and the roughness of the specimen does not change qualitatively. Therefore, the friction angle of the specimen can be considered constant [48]. Therefore, with reference to the relevant research on the same rock [49], we determine the parameters of a more reasonable value. Strain rate is the real-time strain rate obtained from the SHPB dynamic uniaxial compression test. The values of various parameters are shown in Table. 2.

In order to verify the feasibility and adaptability of the damage constitutive relationship, substituting test data and related parameters into the model, the theoretical estimation curve and measured curve carried out in this paper are showed in Fig.14. As reflected in Fig.14, the theoretical fitting curve obtained by the damage constitutive relation is better before the peak point, while after the peak point, the fitting effect is

TABLE 2. Model parameters of specimen at various temperatures.

$T(°C)$	$E\,/\,(GPa)$	$\varphi\,/\,(°)$	η	m	F_0	$\dot{\varepsilon}\,/\,(s^{-1})$
25	43.68	43	0.2	1.42	311.51	140.5
200	42.60	43	0.2	1.23	291.67	192.8
400	58.82	43	0.2	1.64	226.22	40.5
600	17.15	43	0.2	1.76	225.71	92.7
800	6.27T	43	0.2	2.57	108.09	124.2

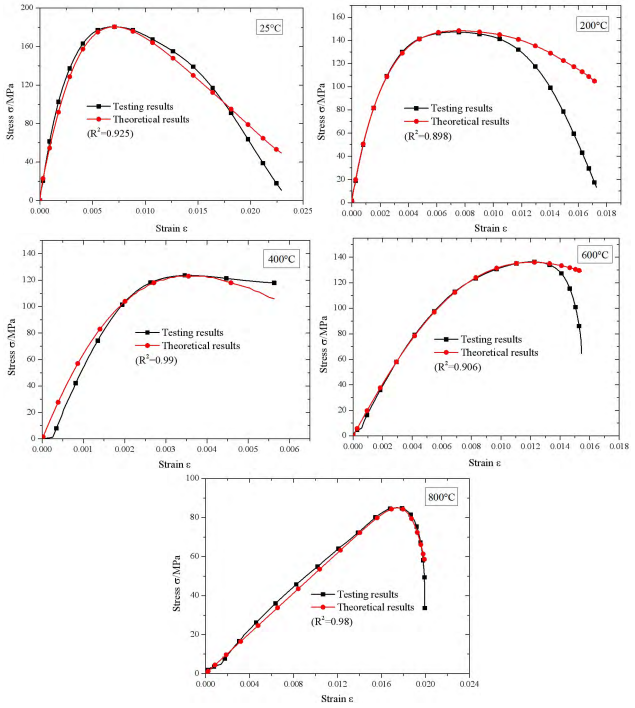

FIGURE 14. Theoretical curves and test curves after different temperatures.

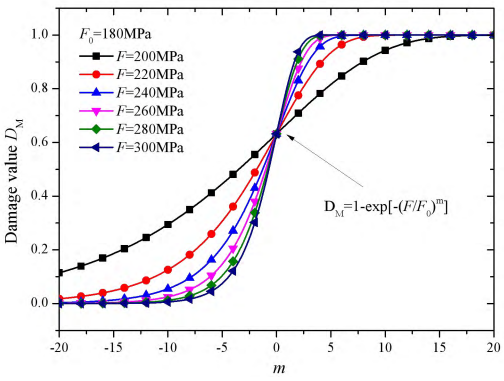

FIGURE 15. The influence of model parameter m on damage in the process of impact load.

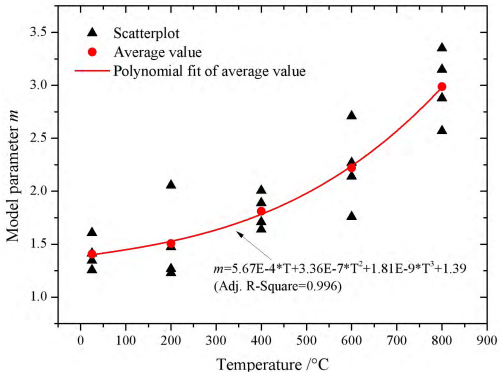

FIGURE 16. The variation of model parameter m with temperature.

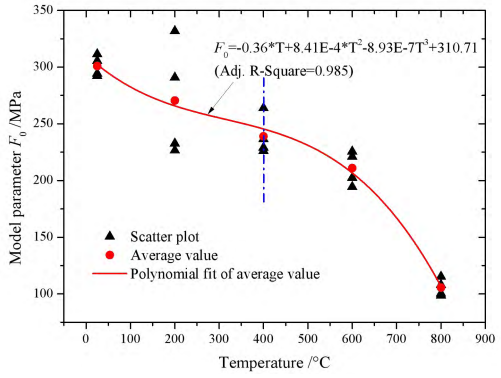

FIGURE 17. The variation of model parameter F_0 with temperature.

relatively poor, but on the whole, the stress–strain curve of the rock sample is well restored. And from the above picture, we also find a problem that cannot be ignored, namely that after the 400°C treatment, the compression stage of the rock sample appears again just like the static condition.

On the other hand, F_0 and m are the two important parameters of Weibull distribution, which can reflect the physical and mechanical properties of rock. In the rock damage model, parameter F indicates the strength of rock micro elements. Strength of rock micro element is always higher than its overall strength, owing to the existence of microscopic defects in the rock mass. Assuming that the dynamic loading of rock under the action of $F_0 = 180$MPa, when the model parameter m increases gradually, the damage value of rock under the different micro element strength were respectively calculated according to Formula (11), as showed in Figure 15.

It could be observed that the damage value of rock gradually increases with the increase of the m value, which indicates that the increase of the model parameter m represents the gradual initiation, penetration and nucleation of micro cracks in the rock during impact loading. For the same strength microelement, the greater the m value of the model parameter, the higher the damage value. Therefore, the model parameter m can be regarded as a non-uniformity value representing the degree of damage inside the rock. It could be observed from Fig.16 that the model parameter m keeps a sustained growth with temperature, which indicates that the thermal treatment effectively weakens the sandstone specimens.

Figure 17 gives the variation of model parameter F_0 with temperature. It is worth noting that the parameter F_0 shows a continued decrease with treatment temperature and the curve descending law is very similar to that of rock dynamic strength with temperature, which indicates that the parameter F_0 can represent the dynamic strength characteristics of rock.

V. DISCUSSION

The foregoing presents a coupled thermal-mechanical dynamic statistical damage constitutive model, in which it is

assumed that the real rock medium is composed of microscopic elements (REVs) and that each of these microscopic elements contains an ensemble of randomly distributed and orientated micro-cracks. Based on the established constitutive model, we now conduct an in-depth discussion. It should be pointed out that the maximum strain is equal to the sum of the plastic strain and the elastic strain, but the elastic strain can be recovered, the residual strain is irreversible, Hooke's law applies only to the linear elastic range, and the fatigue loading after the peak obviously exceeds the linear elasticity Scope, therefore, this article still has some limitations in determining the damage worthwhile, and in fact magnifies the actual damage value, but the model proposed by the author still describes the damage evolution rule of sandstone to a certain extent, and achieves a more ideal effect.

A. IDENTIFICATION OF CRITICAL DAMAGE POINTS

As we all know, under the continuous loading, the primary cracks in the rock sample are first closed and then subjected to the elastic phase at the macro level, and at the end of this stage, secondary cracks begin to appear, that is, the damage threshold is reached. To this end, domestic and overseas scholars have done a lot of work. Martin and Chandler [50], through the study of Lac du Bonnet granite, proposed a crack strain model method to determine the rock initiation stress, and found that the starting stress is 40% of peak strength. However, on the other hand, we know that rock-like materials are not the ideal elastic body, so in the macro elastic stage a certain number of micro-cracks are still produced. Therefore, in the strict sense, it can be considered that the tail of the compression stage is where the damage begins and this is the damage threshold. When it comes to dynamic loads, the initial stress point causing rock damage is more difficult to obtain only from the stress–strain curves.

In this paper, high speed camera is used to record the whole failure process of rock loading, the failure state corresponding to the special point of rock dynamic stress-strain curve is analyzed, as showed in Fig. 18. It could be observed from Fig. 18(a), at room temperature, rock firstly presents elastic deformation characteristics, and the stress-strain curve is approximately a straight line segment, and macroscopic cracks begin to be appeared at 74μs. With the increase of loading time, the enlarged dimension increases, and gradually penetrates the rock specimen. At 120μs, dynamic peak strength is reached, but the failure is not completely ended. Rock fragmentation after the peak is more intense, indicating that the rock has certain bearing capacity after the peak strength.

When the treatment temperature rises to 800 °C, larger thermal damage is produced inside rock. During the initial stage of dynamic loading, rock has undergone great deformation, but no obvious cracks were observed on the rock surface before 100μs. With the increase of loading time, macro-cracks gradually appeared on the surface of rock at 160μs, and the cracks propagate and penetrate rapidly, which eventually lead to rock crushing failure. After high temperature

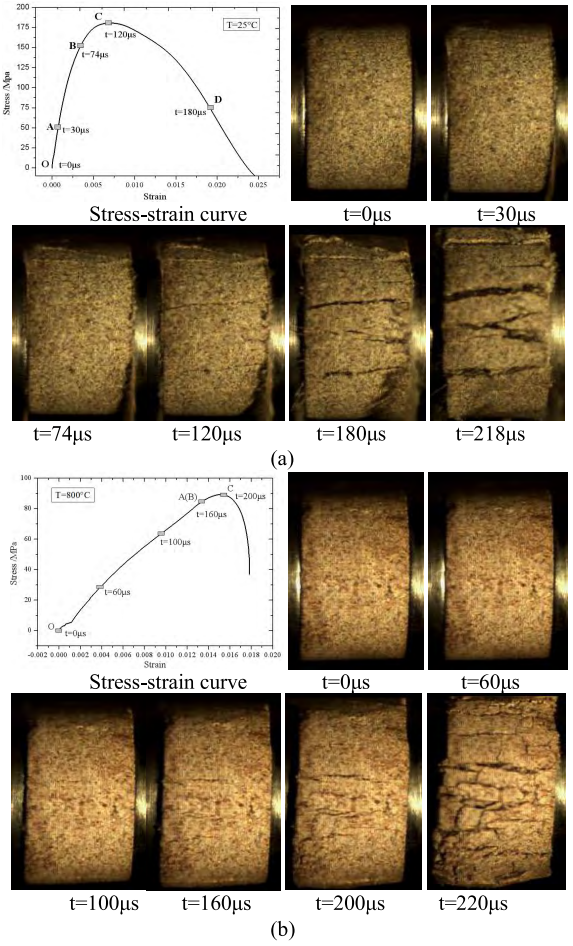

FIGURE 18. Dynamic failure process corresponding to stress-strain curves of sandstone after heat treatment. (a) T = 25°C. (b) T = 800°C.

treatment, the time of rock reaching peak strength and the macroscopic cracks appearing time is all lag behind the normal temperature condition, which indicating that the brittle-plastic transition has been occurred due to high temperature treatment.

Combing damage evolution characteristics and rock failure process recorded by high-speed camera, the dynamic stress-strain relation curves of rock under different temperature can be divided into different variation stages, showed in Fig.19. It could be observed that the axial compressive intensity falls behind the damage evolution rate reaching to the peak point, for which the rock sample is in the plastic zone when the damage rate is at maximum. Almost no mechanical damage occurs in the first stage (OA section), while the total damage is thermal, and A can be seen as the initial point of mechanical damage. At this stage, the rock samples are in the compaction and linear elasticity stage, and almost no new micro-cracks are produced under the action of axial load. The damage curve is at the approximate horizontal extension especially at high temperature. When developing to the second stage (AB section), the damage value increases steadily, and B is the beginning of the plastic stage of the rock specimen,

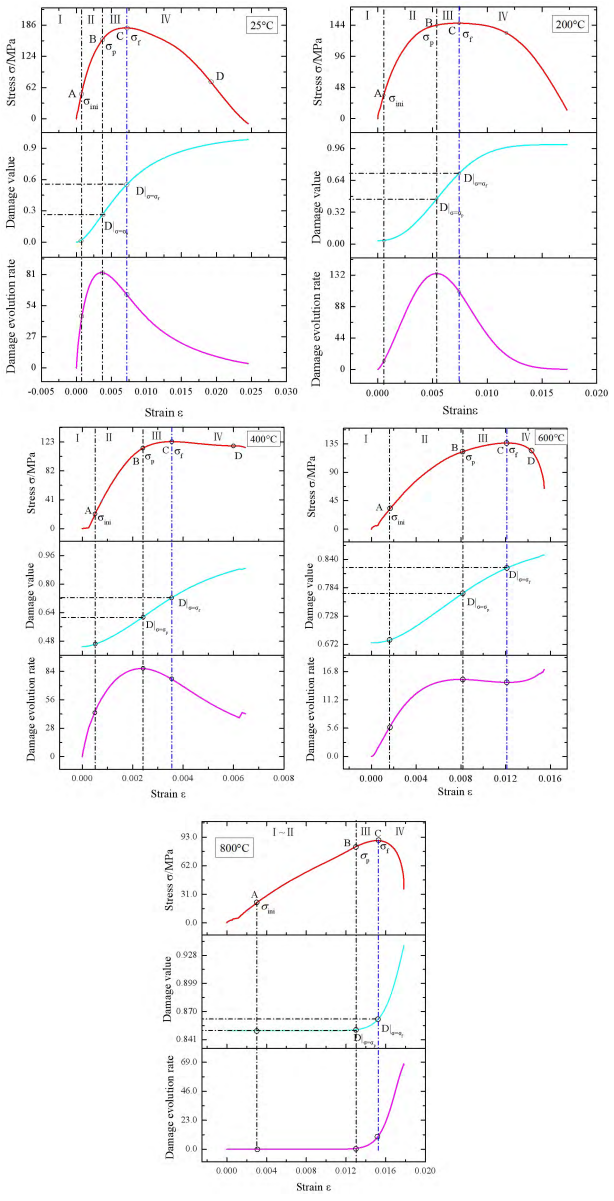

FIGURE 19. Stress-strain and damage evolution curves under different temperatures.

corresponding to the maximum damage evolution rate. Indeed, there is no strict distinction between the elastic phase and the plastic stage, and it is more accurate to consider point B as the end point of the elastic phase. For this stage, the rock enters the elastic-plasticity stage. During this process, numbers of micro-cracks are generated, but there is no larger crack or only a very small number of larger cracks are formed.

The coupled damage of the rock samples shows continuous growth in the third stage (BC section), and C is the peak strength. Along with this developing process, micro-cracks are formed in large quantities, accumulating and expanding through, and eventually leading to macro-structural destruction, which causes the damage value and evolution rate to increase significantly. When the rock specimen strength exceeds the peak intensity, it enters the fourth stage (CD section). Its internal structure is destroyed, but the specimen basically keeps its whole shape. Fissures rapidly develop, intersect and form a macroscopic fracture surface, leading to a rapid decrease of the bearing capacity of the rock specimen. After that, the deformation of the rock is mainly manifested as the slip of the macroscopic fracture surface, and the bearing capacity of the specimen decreases rapidly with the rapid deformation until the residual strength is reached. The damage evolution rate decreases rapidly as the main fracture of the rock has already formed, but the total damage continues to increase until it approaches saturation.

B. DAMAGE EVOLUTION CHARACTERISTICS

It could be observed from Fig. 19 that the values of thermo-mechanical damage increase exponentially with rock strain, and the damage evolution rate presents a two stage variation of first increase and then decrease. At the beginning of the unstable development of rock microcracks, the damage rate reaches the maximum. In addition, it should be noted that when the treatment temperature reaches 800 °C, the damage evolution curve of rock will not follow the three-stage growth law. At the initial stage of loading, with the large deformation increases, the damage value of the rock did not increase significantly. When the deformation reaches the yield strain of rock, the damage value begins increasing exponentially until the rock crushing failure occurs. The main reason for this phenomenon might be that the high temperature effects have caused a large damage inside the rock (from the damage curve, the thermal damage value is approximately 0.85), resulting in loose internal structure and increased ductility.

Table 3 gives the damage and mechanical values of specimen at various temperatures, in which σ_{ini} is the

TABLE 3. Damage and mechanical values of specimen at various temperature.

$T(°C)$	$\sigma_{ini}(MPa)$	$\sigma_p(MPa)$	$\sigma_f(MPa)$	$\sigma_{ini}/\sigma_f(\%)$	$D\big\|_{\sigma=\sigma_p}$	$D\big\|_{\sigma=\sigma_f}$
25	48.26	156.46	180.52	26.73	0.273	0.556
200	37.23	144.24	147.18	25.29	0.461	0.580
400	22.25	114.42	123.65	17.99	0.615	0.723
600	32.03	122.58	136.44	23.48	0.773	0.822
800	21.77	83.07	89.27	24.39	0.852	0.862

stress corresponding to the initial point of damage; σ_p is the stress at the beginning of the unstable stage of microcrack development; σ_f is the dynamic peak stress at different temperatures; σ_{ini}/σ_f is the ratio of initial damage stress to the dynamic peak stress at different temperatures; $D|_{\sigma=\sigma_p}$ and $D|_{\sigma=\sigma_f}$ are respectively the damage value corresponding to the stress of σ_p and σ_f.

It could be observed from Table 3 that the initial damage threshold value decreases with the rise of the treatment temperature, but it can be deduced as about 23% of the peak stress of the rock specimen. When the stress-strain curve is increased to the peak stress, rock damage value does not reach the maximum value of 1, which are respectively 55.6%, 58.0%, 72.3%, 82.2% and 86.2%, indicating that the rock still able to withstand a certain amount of external load and the mechanical damage would be continues to increase in the post peak loading stage. The findings of this paper can provide a reference for the macroscopic mechanical damage of rock under high temperatures of rock in the future.

C. SOME OTHER ISSUES THAT NEED TO BE EMPHASIZED

Based on the study presented in the previous sections, it is clear that an increase in temperature had a significant influence on the physical and mechanical properties of the sandstone. This could be attributed to the thermal stresses induced by the variation of the minerals composition and structural changes within the sandstone.

Since the velocity of ultrasonic waves is directly related to the porosity, density and internal micro-fractures of the media through which they pass, when rocks undergo heat treatment, the distribution of the internal structure of the rock will change greatly. When the P-waves pass through the rock, the initial crack and other thermal stress cracks in the rock give the wave velocity a certain attenuation. Therefore, the variation of wave velocity can also reflect the degree of damage to the internal structure of the rock. In this paper, the ultrasonic wave velocity was taken as a bridge to study the relationship between thermal damage and temperature. This method of defining the damage variable is used for our constitutive model, which can fully reflect the relationship between the strength of the rock and the strain. Furthermore, the rationality of the model is also successfully verified. But there are also some deviations between the model curve and the measured curves, and the rheological effect and frictional force among the internal structures of rock cannot be ignored after the peak intensity. Therefore, in order to establish a more reasonable statistical constitutive model for thermal damage of rock, it is necessary to revise the damage variables based on the post-peak residual strength. This aspect will be studied in the future.

VI. CONCLUSION

This paper analyzed the rules of the changes in the physical and mechanical properties of sandstone in wave velocity and dynamic compressive strength after high temperature preheating, and discussed the internal mechanisms from the micro aspects. Furthermore, in order to better explain the properties of sandstone, we established a dynamic damage statistical constitutive model which considered the temperature effect. Some preliminary conclusions can be drawn as follows:

(1) Thermal treatment effectively weakens the sandstone specimens. The ultrasonic velocity, static and dynamic compression strength of specimen after heat-treatment reduces significantly. The thermal damage of rock represented by longitudinal wave velocity keeps a sustained growth with temperature.

(2) A damage model using the continuum and statistical damage mechanics for sandstone subjected to different temperatures was established, and illustrated the relationship between the degree of rock damage and the related temperature variation.

(3) The proposed model agrees with the test results, indicating that the applicability and reliability of this model can reflect the damage properties and constitution relationship of sandstone in the coupled stress–temperature load. The laboratory tests results and this proposed model can provide an in-depth understanding of the mechanical properties of rocks subjected to coupled stress–temperature load and provide a reference for related engineering practices.

(4) Combining the characteristics of stress-strain curves and damage evolution process of rocks, it was obtained that the values of thermo-mechanical damage increase exponentially with rock strain, and the damage evolution rate presents a two stage variation of first increase and then decrease. At the beginning of the unstable development of rock microcracks, the damage rate reaches the maximum.

(5) During the dynamic loading process, the initial damage threshold value decreases with the rise of the treatment temperature, but it can be deduced as about 23% of the peak stress of the rock specimen. Although the damage value at the peak point of stress increases with the increase of the treatment temperature, it did not reach the maximum value of 1, which indicate that the rock damage continues to increase in the post peak loading stage.

REFERENCES

[1] M. C. He, H. P. Xie, S. P. Peng, and Y. D. Jiang, "Study on rock mechanics in deep mining engineering," *Chin. J. Rock Mech. Eng.*, vol. 24, no. 16, pp. 2803–2813, Aug. 2005.

[2] J. Zhao, "Geothermal testing and measurements of rock and rock fractures," *Geothermics*, vol. 23, no. 3, pp. 215–231, Jun. 1994.

[3] F. E. Heuze, "High-temperature mechanical, physical and thermal properties of granitic rocks—A review," *Int. J. Rock Mech. Mining Sci. Geomechanics Abstr.*, vol. 20, no. 1, pp. 3–10, Feb. 1983.

[4] R. D. Dwivedi, R. K. Goel, V. V. R. Prasad, and A. Sinha, "Thermo-mechanical properties of Indian and other granites," *Int. J. Rock Mech. Mining Sci.*, vol. 45, no. 3, pp. 303–315, Mar. 2008.

[5] M. Hajpál, "Changes in sandstones of historical monuments exposed to fire or high temperature," *Fire Technol.*, vol. 38, no. 4, pp. 373–382, Oct. 2002.

[6] G. Wu, Y. Wang, G. Swift, and J. Chen, "Laboratory investigation of the effects of temperature on the mechanical properties of sandstone," *Geotechn. Geolog. Eng.*, vol. 31, no. 2, pp. 809–816, Apr. 2013.

[7] F. Homand-Etienne and R. Houpert, "Thermally induced microcracking in granites: Characterization and analysis," *Int. J. Rock Mech. Mining Sci. Geomechanics Abstr.*, vol. 26, no. 2, pp. 125–134, Mar. 1989.

[8] L. L. N. Mambou, J. Ndop, and J.-M. B. Ndjaka, "Modeling and numerical analysis of granite rock specimen under mechanical loading and fire," *J. Rock Mech. Geotechnical Eng.*, vol. 7, no. 1, pp. 101–108, Feb. 2015.

[9] G. Shabbir, M. Maqsood, A. Maqsood, I. U. Haq, N. Amin, and S. E. Gustafsson, "Thermophysical properties of rock marbles as a function of temperature," *J. Phys. D, Appl. Phys.*, vol. 26, no. 10, pp. 1576–1580, Jan. 1993.

[10] V. Rocchi, P. R. Sammonds, and C. R. J. Kilburn, "Fracturing of Etnean and Vesuvian rocks at high temperatures and low pressures," *J. Volcanol. Geothermal Res.*, vol. 132, nos. 2–3, pp. 137–157, Apr. 2004.

[11] H. Yavuz, S. Demirdag, and S. Caran, "Thermal effect on the physical properties of carbonate rocks," *Int. J. Rock Mech. Mining Sci.*, vol. 47, no. 1, pp. 94–103, Jan. 2010.

[12] U. S. Lindholm, L. M. Yeakley, and A. Nagy, "The dynamic strength and fracture properties of dresser basalt," *Int. J. Rock Mech. Mining Sci. Geomechanics Abstr.*, vol. 11, no. 5, pp. 181–191, May 1974.

[13] T. Yin, X. Li, W. Cao, and K. Xia, "Effects of thermal treatment on tensile strength of laurentian granite using brazilian test," *Rock Mech. Rock Eng.*, vol. 48, no. 6, pp. 2213–2223, Feb. 2015.

[14] T. Yin, P. Wang, X. Li, B. Wu, M. Tao, and R. Shu, "Determination of dynamic flexural tensile strength of thermally treated Laurentian granite using semi-circular specimens," *Rock Mech. Rock Eng.*, vol. 49, no. 10, pp. 3887–3898, Feb. 2016.

[15] X. B. Li, T. S. Lok, J. Zhao, and P. J. Zhao, "Oscillation elimination in the Hopkinson bar apparatus and resultant complete dynamic stress–strain curves for rocks," *Int. J. Rock Mech. Mining Sci.*, vol. 37, no. 7, pp. 1055–1060, Oct. 2000.

[16] D. J. Frew, M. J. Forrestal, and W. Chen, "A split Hopkinson pressure bar technique to determine compressive stress-strain data for rock materials," *Exp. Mech.*, vol. 41, no. 1, pp. 40–46, Mar. 2001.

[17] K. Bian, J. Liu, W. Zhang, X. Zheng, S. Ning, and Z. Liu, "Mechanical behavior and damage constitutive model of rock subjected to water-weakening effect and uniaxial loading," *Rock Mech. Rock Eng.*, pp. 1–10, Aug. 2018, doi: 10.1007/s00603-018-1580-4.

[18] Z. L. Wang, H. Shi, and J. G. Wang, "Mechanical behavior and damage constitutive model of granite under coupling of temperature and dynamic loading," *Rock Mech. Rock Eng.*, vol. 51, no. 10, pp. 3045–3059, Oct. 2018, doi: 10.1007/s00603-018-1523-0.

[19] E. Hoek, and E.T. Brown, *Underground Excavations in Rock*. London, U.K.: Institute of Mining and Metallurgy, 1980.

[20] S. Priest, "Three-dimensional failure criteria based on the Hoek–Brown criterion," *Rock Mech. Rock Eng.*, vol. 45, no. 6, pp. 989–993, Nov. 2012.

[21] Q. Zhang, H. Zhu, and L. Zhang, "Modification of a generalized three-dimensional Hoek–Brown strength criterion," *Int. J. Rock Mech. Mining Sci.*, vol. 59, pp. 80–96, Apr. 2013.

[22] X. S. Liu, J. G. Ning, Y. L. Tan, and Q. H. Gu, "Damage constitutive model based on energy dissipation for intact rock subjected to cyclic loading," *Int. J. Rock Mech. Mining Sci.*, vol. 85, pp. 27–32, May 2016.

[23] C. Wen-Gui, L. Xiang, and Z. Heng, "Damage constitutive model for strain-softening rock based on normal distribution and its parameter determination," *J. Central South Univ. Technol.*, vol. 14, pp. 719–724, Oct. 2007.

[24] D. Krajcinovic and M. A. G. Silva, "Statistical aspects of the continuous damage theory," *Int. J. Solids Struct.*, vol. 18, no. 7, pp. 551–562, Dec. 1982.

[25] L. M. Yang and V. P. W. Shim, "An analysis of stress uniformity in split Hopkinson bar test specimens," *Int. J. Impact Eng.*, vol. 31, no. 2, pp. 129–150, Feb. 2005.

[26] S. Liu and J. Y. Xu, "Analysis on damage mechanical characteristics of marble exposed to high temperature," *Int. J. Damage Mech.*, vol. 24, no. 8, pp. 1180–1193, Feb. 2015.

[27] N. Barton, "Suggested methods for the quantitative description of discontinuities in rock masses: International society for rock mechanics," *Int. J. Rock Mech. Mining Sci. Geomechanics Abstr.*, vol. 15, no. 6, pp. 319–368, Jan. 1978.

[28] Y. X. Zhou *et al.*, "Suggested methods for determining the dynamic strength parameters and mode-I fracture toughness of rock materials," *Int. J. Rock Mech. Mining Sci.*, vol. 49, pp. 105–112, Jan. 2012.

[29] M. H. B. Nasseri, A. Schubnel, and R. P. Young, "Coupled evolutions of fracture toughness and elastic wave velocities at high crack density in thermally treated Westerly granite," *Int. J. Rock Mech. Mining Sci.*, vol. 44, no. 4, pp. 601–616, Jun. 2007.

[30] T. Yin, L. Bai, X. Li, and S. Zhang, "Effect of thermal treatment on the mode I fracture toughness of granite under dynamic and static coupling load," *Eng. Fracture Mech.*, vol. 199, pp. 143–158, Aug. 2018.

[31] P. Wang, T. Yin, X. Li, S. Zhang, and L. Bai, "Dynamic properties of thermally treated granite subjected to cyclic impact loading," *Rock Mech. Rock Eng.*, pp. 1–20, Oct. 2018, published online, doi: 10.1007/s00603-018-1606-y.

[32] T. Yin, S. Zhang, X. Li, and L. Bai, "A numerical estimate method of dynamic fracture initiation toughness of rock under high temperature," *Eng. Fract. Mech.*, vol. 204, pp. 87–102, Dec. 2018.

[33] X. B. Li, T. S. Lok, and J. Zhao, "Dynamic characteristics of granite subjected to intermediate loading rate," *Rock Mech. Rock Eng.*, vol. 38, no. 1, pp. 21–39, Jan. 2005.

[34] Z. Zhou, X. Li, Z. Ye, and K. Liu, "Obtaining constitutive relationship for rate-dependent rock in SHPB tests," *Rock Mech. Rock Eng.*, vol. 43, no. 6, pp. 697–706, Nov. 2010.

[35] X. Li, Z. Zhou, T.-S. Lok, L. Hong, and T. Yin, "Innovative testing technique of rock subjected to coupled static and dynamic loads," *Int. J. Rock Mech. Mining Sci.*, vol. 45, no. 5, pp. 739–748, Jul. 2008.

[36] Z. Zhou, X. Li, A. Liu, and Y. Zou, "Stress uniformity of split Hopkinson pressure bar under half-sine wave loads," *Int. J. Rock Mech. Mining Sci.*, vol. 4, no. 48, pp. 697–701, Jun. 2010.

[37] P. Y. Zhu, D. S. Liu, Y. D. Peng, and A. H. Chen, "Inverse approach to determine piston profile from impact stress waveform on given non-uniform rod," *Trans. Nonferrous Met. Soc. China*, vol. 11, no. 2, pp. 297–300, Apr. 2001.

[38] F. Dai, S. Huang, K. Xia, and Z. Tan, "Some fundamental issues in dynamic compression and tension tests of rocks using split Hopkinson pressure bar," *Rock Mech. Rock Eng.*, vol. 43, no. 6, pp. 657–666, Nov. 2010.

[39] Q. B. Zhang and J. Zhao, "A review of dynamic experimental techniques and mechanical behaviour of rock materials," *Rock Mech. Rock Eng.*, vol. 47, no. 4, pp. 1411–1478, Jul. 2013.

[40] T. B. Yin, X. Li, K. Xia, and S. Huang, "Effect of thermal treatment on the dynamic fracture toughness of Laurentian granite," *Rock Mech. Rock Eng.*, vol. 45, no. 6, pp. 1087–1094, May 2011.

[41] J. Lemaitre, "How to use damage mechanics," *Nucl. Eng. Des.*, vol. 80, no. 2, pp. 233–245, Jul. 1984.

[42] E. Rossi, M. A. Kant, C. Madonna, M. O. Saar, and P. R. von Rohr, "The effects of high heating rate and high temperature on the rock strength: Feasibility study of a thermally assisted drilling method," *Rock Mech. Rock Eng.*, vol. 51, no. 9, pp. 2957–2964, 2018, doi: 10.1007/s00603-018-1507-0.

[43] X. Li, S.-M. Wang, L. Weng, L.-Q. Huang, T. Zhou, and J. Zhou, "Damage constitutive model of different age concretes under impact load," *J. Central South Univ.*, vol. 22, no. 2, pp. 693–700, Feb. 2015.

[44] K. Li and J.-L. Tao, "High temperature dynamic constitutive relation of concrete-like brittle material," in *Proc. IEEE Int. Conf. Electric Technol. Civil Eng.*, Apr. 2011, pp. 417–421.

[45] J. Lemaitre, "A continuous damage mechanics model for ductile fracture," *J. Eng. Mater. Technol.*, vol. 107, no. 1, pp. 83–89, Jan. 1985.

[46] H. M. Zhang and G. S. Yang, "Research on damage model of rock under coupling action of freeze-thaw and load," *Chin. J. Rock Mech. Eng.*, vol. 29, no. 3, pp. 471–476, Mar. 2010.

[47] Q. Zhang, G. Yang, and J. Ren, "New study of damage variable and constitutive equation of rock," *Chin. J. Rock Mech. Eng.*, vol. 22, no. 1, pp. 30–34, Jan. 2003.

[48] C. B. Xu and H. S. Zhou, "Test investigation of triaxial compressive strength of coarse sandstone after high temperature," *Chin. J. Rock Mech. Eng.*, vol. 35, no. Supp.1, pp. 2811–2818, May 2016.

[49] F. Q. Gong, D. H. Lu, X. B. Li, and Q. H. Rao, "Experimental research of sandstone dynamic strength criterion under different strain rates," *Rock Soil Mech.*, vol. 34, no. 9, pp. 2433–2441, Sep. 2013.

[50] C. D. Martin and N. A. Chandler, "The progressive fracture of Lac du Bonnet granite," *Int. J. Rock Mech. Mining Sci. Geomechanics Abstr.*, vol. 31, no. 6, pp. 643–659, Dec. 1994.

TUBING YIN received the Ph.D. degree from the School of Resources and Safety Engineering, Central South University, Changsha, China, in 2012. From 2009 to 2012, he was a Visiting Scholar with Toronto University, Canada. He has authored over 50 papers published in academic journals, and 14 national invention patents. His current research interests include rock dynamics, damage characteristics of rock materials, mechanics of rock under high temperature and high pressure conditions, and some rock/mineral mechanics for deep mining science.

He is currently an Associate Professor with the School of Resources and Safety Engineering, Central South University. He is a member of the Rock Dynamic Commission of the Chinese Society for Rock Mechanics and the Executive Member of the Hunan Province Society for Rock Mechanics and Engineering. He received the First Prize of Science and Technology Award of China Gold Association three times, the First Prize of Science and technology Award of China Nonferrous Metals Industry, the Provincial Excellent Doctor Degree Dissertation, and three other ministerial level awards. He has served as a reviewer of more than 30 journals.

PIN WANG received the M.Sc. degree in mining engineering from Central South University, Changsha, China, in 2017, where he is currently pursuing the Ph.D. degree. His research interests include rock dynamics, damage characteristics of rock material, mechanics of rock under high temperature condition, and the constitutive relationship of rocks under high strain rates.

JIAN YANG received the B.Sc. degree in safety science engineering from Henan Polytechnic University, Jiaozuo, China, in 2016. He is currently pursuing the M.Sc. degree in safety science engineering with Central South University. His research interests include rock mechanics, structural stability of rock mass and the safety of production, and the constitutive relationship of rocks under high strain rates.

XIBING LI received the Ph.D. degree in mining engineering from the Central South University of Technology, Changsha, China, in 1992. He was a Senior Visiting Scholar with the Rock Mechanics and Explosives Research Center, University of Missouri-Rolla, from 1998 to 1999. He was also a Researcher with Nanyang Technological University, Singapore, from 1999 to 2001. He received four projects of National Science and Technology Awards, and 14 projects of Provincial/Ministerial Science and Technology Awards. He was selected for the National Science Fund for Distinguished Young Scholars and a Chang Jiang Distinguished Professor. He received awards, including the National Award for Youth in Science and Technology and the National Excellent Scientific and Technological Worker.

Dr. Li has been a Committee Member of the Rock Dynamics of International Society for Rock Mechanics since 2008. He has also been the Vice President of the Chinese Society for Rock Mechanics and Engineering since 2016.